ROYAL SOCIETY
OF CHEMISTRY

PAPER

Check for updates

First-principles studies of a two-dimensional electron gas at the interface of polar/polar LaAlO₃/KNbO₃ superlattices†

Le Fang, [ID] [abc] Chen Chen, [ab] Yali Yang, [ab] Yabei Wu, [ab] Tao Hu, [ID] [ab] Guodong Zhao, [ID] [ab] Qiang Zhu [ID] [c] and Wei Ren [ID] ★[ab]

We explored the possibility of producing a two-dimensional electron gas (2DEG) in polar/polar $(LaAlO_3)_m/(KNbO_3)_n$ perovskite superlattices that have N type and P type interfaces using the first-principles electronic structure calculations. Two different kinds of LaAlO₃/KNbO₃ superlattices were constructed, namely stoichiometric NP superlattice (NP-SL) and non-stoichiometric NN superlattice (NN-SL). We discovered that the NP-SL undergoes a transition from an insulating to a metallic state when LaAlO₃ has more than 3 unit cells. This reveals the completely spin-polarized two-dimensional hole gas (2DHG), as well as 2DEG with an interfacial charge carrier density of $n \sim 10^{13}$ cm^{-2} and an electron effective mass of $0.240m_e$ (for 5 unit cells of LaAlO₃). In comparison, the NN-SL is intrinsically metallic, and when LaAlO₃ has 4.5 unit cells, the structure shows a 2DEG with a larger density ($n \sim 10^{14}$ cm^{-2}) and a smaller electron effective mass ($0.185m_e$). In addition, the charge carrier properties are highly sensitive to the number of LaAlO₃ unit cells in the NP-SL model, while the size effect of LaAlO₃ is negligible for the NN-SL one. Our results demonstrate that electronic reconstruction at the interfaces of the stoichiometric structure can produce both the 2DHG and 2DEG, whereas extra electrons are introduced to form solely the 2DEG at the non-stoichiometric structure interfaces. This research provides fundamental insights into the different interfacial electronic properties and the primary mechanism responsible for the formation of polar/polar heterojunction LaAlO₃/KNbO₃ superlattices.

1. Introduction

A two-dimensional electron gas (2DEG) can be generated at the interfaces of perovskite-based oxide heterostructures or super-lattices with novel characteristics,[1] and has attracted lots of attention. The 2DEG has been suggested for use in next-generation nano-electronic oxide devices because of its unique electronic properties, such as ferroelectric polarization enhancement,[2] high charge carrier mobility,[3] two-dimension superconductivity,[4] magnetism at the interface,[5] electronic spin polarization,[6,7] and so on. A well-studied example is the formation of the 2DEG in a polar/nonpolar interface system composed of two oxide insulators LaAlO₃/SrTiO₃ (LAO/STO).[8]

There are many proposed scenarios that explain the fascinating formation of the 2DEG. Electronic reconstruction is considered to be an effective approach to obtain the 2DEG at the heterojunction interface of perovskite oxides.[9] In general, perovskites have a chemical formula of $A^{X+}B^{Y+}O_3$ (where $X + Y = 6$), and they contain alternating planes of $(A^{X+}O^{2-})$ and $(B^{Y+}O_2^{2-})$ in the [001] direction. Therefore, the alternating planes of AO and BO₂ may be charged (if $X = 1, 3$) or neutral (if $X = 2$), which gives rise to three types of heterojunctions: polar/nonpolar, nonpolar/nonpolar, and polar/polar systems. The LAO/STO system is a typical polar/nonpolar example,[8] where LaAlO₃ (LAO) is composed of atomic planes of alternating charges $(LaO)^+$ and $(AlO_2)^-$, while SrTiO₃ (STO) consists of neutral $(TiO_2)^0$ and $(SrO)^0$ layers along the [001] direction. When LAO is placed on STO in the [001] direction, two kinds of interfaces may exist with combinations of $(LaO)^+/(TiO_2)^0$ and $(AlO_2)^-/(SrO)^0$ planes. As the number of LAO unit cells increases, the polar discontinuity at the interface causes a divergence in the electrostatic potential which will lead to "a polar catastrophe".[4] It is well known that the polar discontinuity of semiconductor heterointerfaces may introduce atomic reconstruction to avoid diverging electrostatic potential.[10,11] However, it is possible to make electronic reconstruction by introducing mixed

[a] *Materials Genome Institute, International Center for Quantum and Molecular Structures, Shanghai University, Shanghai 200444, China. E-mail: renwei@shu.edu.cn*

[b] *Shanghai Key Laboratory of High Temperature Superconductors, Department of Physics, Shanghai University, Shanghai 200444, China*

[c] *Department of Physics and Astronomy, High Pressure Science and Engineering Center, University of Nevada, Las Vegas, NV 89154, USA*

† Electronic supplementary information (ESI) available. See DOI: 10.1039/c8cp07202g

valence for transition metals in perovskites.[12] For the LAO/STO heterostructure,[9] half an electron is transferred from the charged layer $(LaO)^+$ to the neutral layer $(TiO_2)^0$, resulting in a metallic state at the interface of $(LaO)^+/(TiO_2)^0$. Besides, there exist many other factors such as polarization discontinuity,[13] oxygen vacancies,[14] cation intermixing,[15] modulation doping,[16] *etc.*, which also possibly affect the electronic states of the above-mentioned systems.

Compared to the polar/nonpolar heterostructure, in the polar/polar case, both perovskite oxides can donate electrons onto the interface, thus generating a higher interfacial charge carrier density. From the previous work of Zou *et al.*,[17] the polar/polar $LaTiO_3/KTaO_3$ system can be synthesized experimentally to produce the higher mobility 2DEG with smaller effective mass for electrons, because the polar discontinuity has twice the magnitude of the polar/nonpolar heterostructure. Afterwards the polar/polar $LaAlO_3/ABO_3$ (A = Na, K; B = Nb, Ta) systems are studied using the first-principles method by Wang *et al.*[18] In addition, Li *et al.* also have revealed that the polar/polar $LaBO_3/KNbO_3$ (B = Al, Ga) heterostructures generate higher

interfacial carrier density and smaller effective mass than the typical polar/nonpolar LAO/STO system.[19]

The interfacial geometry and hybridization can successfully tune the metal–insulator transition and the 2DEG, providing another effective method to control perovskite insulators.[20] In this work, we chose the polar/polar $LaAlO_3/KNbO_3$ (LAO/KNO) superlattice to analyze the interfacial properties. The choice of LAO and $KNbO_3$ (KNO) has several reasons. First, LAO and KNO both are well studied perovskites and KNO can be a substrate material with polar terminations in contrast to the neutral STO substrate in the typical LAO/STO system. Second, the orbitals of Nb 4d are less localized than those of Ti 3d states, which may result in a larger charge carrier mobility than that in $SrTiO_3$-based systems.[18] Third, the band gap of LAO (5.60 eV)[8] is larger than that of KNO (3.14 eV),[21] resulting in the accumulation of the 2DEG at the KNO side. Two different types of models are preferentially considered in this paper, namely the stoichiometric NP-SL with both interfaces and non-stoichiometric NN-SL with only N type interfaces. The primary mechanism responsible for the formation of 2DEG, the origin of the interfacial metallic states, interfacial charge density, and electron effective mass were thoroughly investigated. This research provides fundamental insights into different interfacial electronic properties, which could be an alternative way to produce the 2DEG at the interface of the polar/polar perovskite-based superlattice.

2. Structural and computational details

KNO is a ferroelectric material with the perovskite structure, and a ferroelectric Curie point of 434 °C.[22] It has a cubic
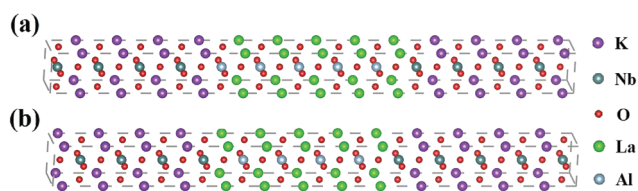
Fig. 1 Atomic structures with the (a) stoichiometric NP type (LaO/NbO_2 and AlO_2/KO interfaces) of $(LaAlO_3)_5/(KNbO_3)_8$ and (b) non-stoichiometric NN type (two LaO/NbO_2 interfaces) of $(LaAlO_3)_{4.5}/(KNbO_3)_{8.5}$ superlattices, respectively.

Fig. 2 The calculated spin-resolved total density of states (DOS) for the stoichiometric $(LaAlO_3)_m/(KNbO_3)_8$ superlattices (m = 2−5). The blue and red lines show the majority-spin and minority-spin states, respectively. The vertical dashed lines at 0 eV indicate the Fermi level.

This journal is © the Owner Societies 2019

Phys. Chem. Chem. Phys., 2019, **21**, 8046–8053 | **8047**

structure with K at (0 0 0), Nb at (0.5 0.5 0.5), and O at (0.5 0.5 0), (0.5 0 0.5), and (0 0.5 0.5) above the Curie temperature, while the lattice constant of KNO is 4.022 Å.[22] LAO exhibits a cubic-rhombohedral phase transition below 540 °C,[23] and the cubic LAO structure has a lattice constant of 3.789 Å.[8] To describe the experimental epitaxial film g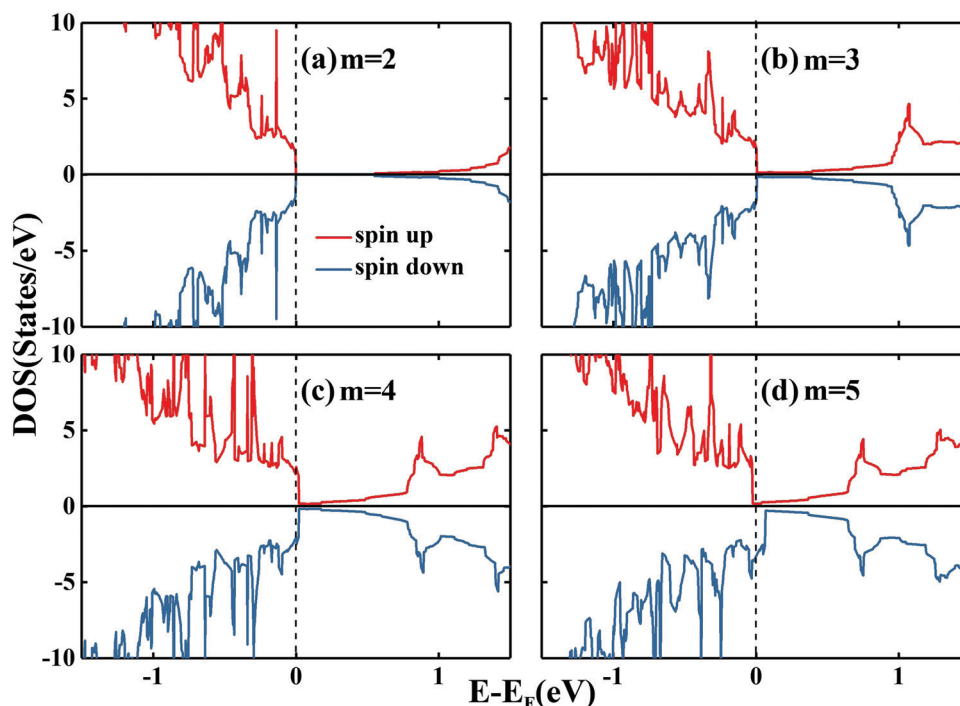rowth, both perovskites are treated approximately as the pseudocubic phase.[24] In the superlattice, the lattice mismatch f between LAO and KNO is 5.79%, as determined by $f = (a_f - a_s)/a_f$, where a_f and a_s are the lattice constants of the epitaxial films LAO and KNO. We fixed the in-plane lattice parameters to be that of KNO, such that LAO is under a tensile strain.[25] It has been successfully reported in experiments that the KNO/LAO epitaxial films can be grown by using the metalorganic chemical vapor deposition.[26,27]

Our electronic structure calculations were based on density functional theory (DFT)[28] as implemented in the Vienna *ab initio* Simulation Package (VASP).[29] Considering the strong correlation effects of Nb 4d and La 4f electrons, we applied the generalized gradient approximation (GGA) parametrized *via* the Perdew–Burke–Ernzerhof (PBE) plus on-site Coulomb interaction approach (PBE+U)[30] in LAO/KNO superlattices, and effective U values of 5 eV[31] and 7.5 eV[32] were used for Nb 4d and La 4f orbitals, respectively. The projected augmented-wave (PAW) method was used to describe the electron–ion interaction. We performed all calculations by employing a cutoff energy of 520 eV[33,34] for the plane wave basis set and a Monkhorst–Pack k-point mesh of $7 \times 7 \times 1$. The superlattice c-axis and the atomic positions were optimized until each atom had a force smaller than 0.01 eV Å^{-1} to resemble the epitaxial growth experiments. The electronic energy convergence was set to 10^{-6} eV in the self-consistent calculations.

Periodic boundary conditions[35,36] are applied while building the (LAO)$_m$/(KNO)$_n$ superlattices *via* stacking the epitaxial slabs along the [001] direction. The KNO lattice constant is used as the substrate. We have also constructed and calculated the freestanding LaAlO$_3$/KNbO$_3$ (LAO/KNO) heterostructures under vacuum by using the same parameters in the text, as shown in Fig. S1 (ESI†). There are N-type and P-type interfaces for heterojunctions, and three types of structures in the LAO/KNO superlattices are constructed: namely NP, NN and PP. As shown in Fig. 1, we fix the number of KNO layers to be 8 or 8.5. When m and n = 8 are both integers, we have the NP structure with negative and positive charged interfaces in the supercell; and when m is a half integral with n = 8.5 the superlattice is of NN type with only positive charged interfaces. The NP configuration maintains the stoichiometry of the superlattice with N-type (LaO)$^+$/(NbO$_2$)$^+$ and P-type (AlO$_2$)$^-$/(KO)$^-$ interfaces, whereas the NN and PP types include double interfaces of N-type (LaO)$^+$/(NbO$_2$)$^+$ and P-type (AlO$_2$)$^-$/(KO)$^-$ in supercells, respectively. These two types are both non-stoichiometric superlattices, in which "extra" electrons or holes are injected into the superlattices. In this work, we focus on the NP and NN superlattices (see in Fig. 1), because PP may involve issues of oxygen vacancies[9] which makes the superlattice more complex and beyond the scope of this research.[37] The interface types can nowadays be precisely controlled by depositing atomic layers in

experiments with the development of advanced layer-by-layer growth techniques.[38]

3. Results and discussion

3.1. The 2DEG in the NP type superlattices

There is a critical layer of 4–6 LAO unit cells which leads to a transition from an insulating to metallic state in the LAO/STO system.[3,6,12,39] We first explored whether there exists such a critical

Fig. 3 (a) The calculated layer-resolved partial DOS for the (LaAlO$_3$)$_5$/(KNbO$_3$)$_8$ superlattice in the range from −3.0 eV to 3.0 eV, along with spin density projected on each oxide monolayers. (b) The orbital-resolved DOS for the Nb atom at the first (IF-1) monolayer and the O atom at the first (IF'-1) monolayer.

8048 | *Phys. Chem. Chem. Phys.*, 2019, **21**, 8046–8053

This journal is © the Owner Societies 2019

LAO thickness to form a conducting state at the interface of the LAO/KNO superlattices. To reveal the dependence of interfacial metallic states on the LAO unit cells, we calculated the total density of states (DOS) for the $(LAO)_m/(KNO)_8$ superlattices (m = 2, 3, 4, 5), as shown in Fig. 2. The superlattice behaves as a semiconductor with a band gap about 0.546 eV for m = 2. While the band gap vanishes for m larger than 3 and the superlattice interface appears to be metallic with small DOS around the Fermi level as shown in Fig. 2(b). The conduction band minimum (CBM) shifts downward and slightly overlaps with the valence band maximum (VBM) with increasing LAO unit cells. Because the polarization decreases as the LAO unit cell increases,[40] which is not enough to fully neutralize the growth divergence of the electrostatic potential with 3 unit cells of LAO, thus the superlattice becomes conducting. In addition, Fig. 2(d) clearly shows that the electronic states become half-metallic like with high spin polarization when m = 5.

To reveal the origin of metallic states and the electron transfer in the stoichiometric polar/polar LAO/KNO superlattices, we calculated layer-resolved partial DOS (PDOS) with the spin charge density of the $(LAO)_5/(KNO)_8$ superlattice, as shown in Fig. 3(a). There are two kinds of interfaces in the superlattice periodic model, $(LaO)^+/(NbO_2)^+$ and $(AlO_2)^-/(KO)^-$ planes. We used IF-1 and IF-2 to represent the first and second NbO_2 monolayers of the $(LaO)^+/(NbO_2)^+$ interface, and IF′-1 and IF′-3 to represent the first and second AlO_2 monolayers as well as IF′-2 to represent the first LaO monolayer.

We found that the electronic reconstruction driven by a polar catastrophe results in a charge transfer from LAO to KNO and accumulates mainly within the $(NbO_2)^+$ monolayer due to the lower CBM of KNO, forming N-type conductivity as captured by the Nb 4d orbitals. Besides, it is clear that O 2p states of the LAO and Nb 4d states of the KNO layers move toward higher energy away from the $(LaO)^+/(NbO_2)^+$ interface because of the electric field caused by the asymmetrical polar layers. Near the $(LaO)^+/(NbO_2)^+$ interface, the occupied Nb 4d states of IF-1 cross the Fermi level, generating metallic states confined to the interface. While near the interface of $(AlO_2)^-/(KO)^-$, the partially occupied O 2p states of IF′-1, IF′-2, IF′-3 cross the Fermi level, generating a completely spin-polarized conductive property. This means that the NP-SL has P-type semiconducting states at the $(AlO_2)^-/(KO)^-$ interface and all the half-metallic states of the $(LAO)_5/(KNO)_8$ superlattice are from O 2p orbitals. Therefore, there is a coexistence of the 2DEG and two-dimensional hole gas (2DHG) in the NP polar/polar LAO/KNO superlattices. Thus such oxide superlattices provide a platform for the exciting physics of confined electron–hole systems and their applications.[33] From the above analysis, the metallic states in Fig. 2 are due to the hybridization effect of Nb 4d and O 2p orbitals, with the overlapping O 2p states and Nb 4d states shifting toward the Fermi energy.

The orbital-resolved partial DOS of Nb 4d orbitals (IF-1) and O 2p orbitals (IF′-1) are shown in Fig. 3(b). There are two types of splitted orbitals in the octahedral crystal field, which are t_{2g} (d_{xy}, d_{yz}, d_{xz}) and e_g (d_{z^2}, $d_{x^2-y^2}$). The three t_{2g} orbitals have a lower energy. In the superlattices, the interfacial NbO_6 octahedron of the $(LaO)^+/(NbO_2)^+$ interface splits three orbitals due to lattice distortion, namely d_{xy}, d_{yz}, d_{xz} orbitals. Because the d_{xy} orbital has a lower energy, it can be occupied first and solely contribute to the metallic states at the IF-1 NbO_2 layer.

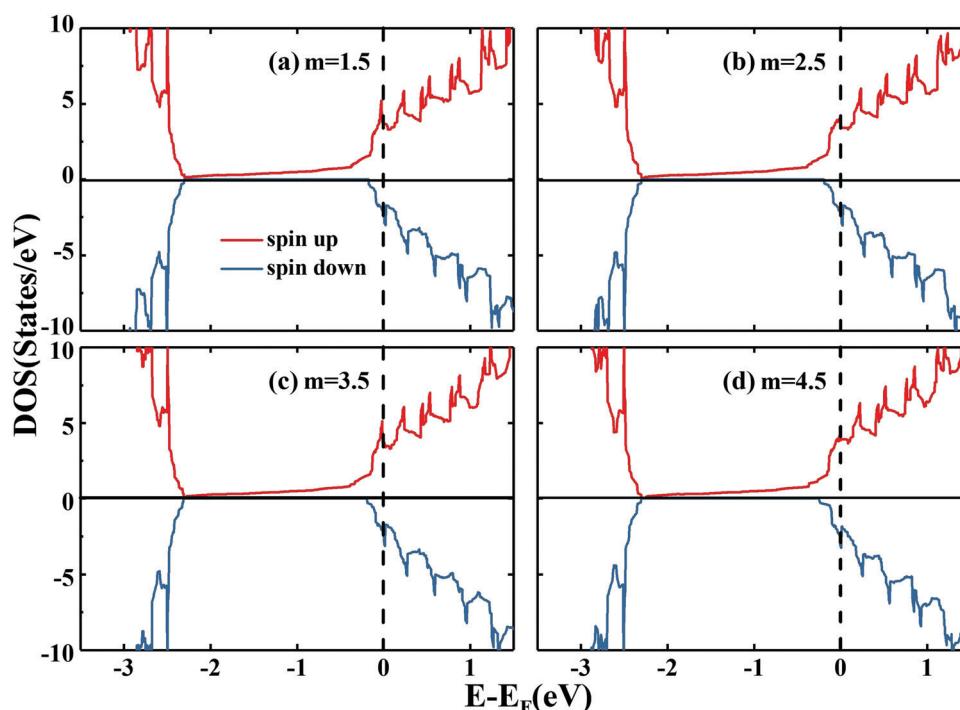**Fig. 4** Calculated spin-resolved total density of states (DOS) for the $(LaAlO_3)_m/(KNbO_3)_{8.5}$ superlattices (m = 1.5, 2.5, 3.5, 4.5). The red and blue lines show the majority-spin and minority-spin DOS, respectively. The vertical lines at 0 eV indicate the Fermi level.
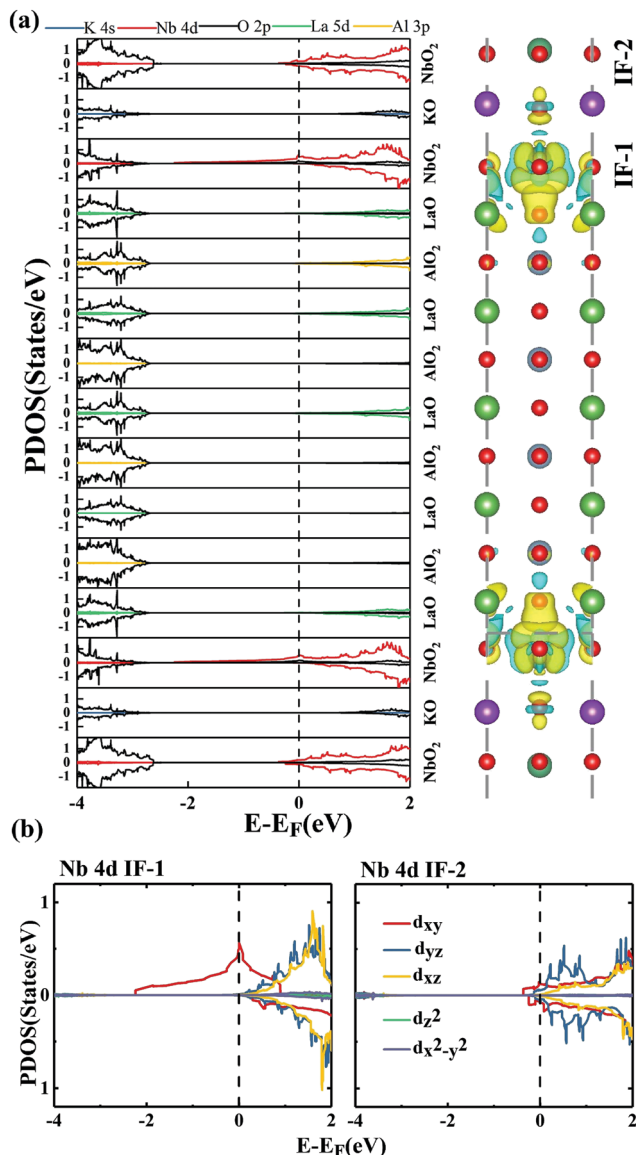
This journal is © the Owner Societies 2019

Phys. Chem. Chem. Phys., 2019, **21**, 8046–8053 | **8049**

(a)

(b)

Fig. 5 (a) The calculated layer-resolved partial DOS for the $(LaAlO_3)_{4.5}/(KNbO_3)_{8.5}$ superlattice in the range from −4.0 eV to 2.0 eV, along with spin density projected on each oxide monolayer. (b) The orbital-resolved DOS for the Nb atom at the first (IF-1) and second (IF-2) monolayers.

In contrast, the d_{yz} and d_{xz} orbitals have higher energy and less occupancy.[41] Therefore, the metallic states at the IF-1 NbO_2 layer are all from $4d_{xy}$ orbitals, while the half metallic states of O 2p states are almost from p_z orbitals and a little part comes from p_x and p_y orbitals for IF′-1.

3.2. 2DEG in the NN type superlattices

For the NP type of LAO/KNO superlattices, the critical layer m is equal to 3, while there is no critical film for the insulator-to-metal transition in NN structures (as shown in the Fig. 4). In other words, it is intrinsically conductive. The total DOS clearly exhibit a typical N-type conductivity, which shows no significant change from $m = 1.5$ to $m = 4.5$. The formation of interfacial conductivity between the NP-SL and NN-SL is different.

For stoichiometric superlattices we expect that the electronic reconstruction driven by a polar catastrophe results in the 2DEG,[26] while it can be explained for the non-stoichiometric NN-SL that "extra" electrons are injected into the system because of uncompensated ionic charges.[42] "Extra" electrons are transferred from the $(LaO)^+$ layer to the $(NbO_2)^+$ layer and captured by the Nb 4d orbitals in order to accommodate such electronic charges, leading to an interfacial 2DEG.

To understand the origin of metallic states and the electron transfer in the NN-SL, we plotted the layer-resolved PDOS of the $(LAO)_{4.5}/(KNO)_{8.5}$ superlattice, as shown in Fig. 5(a). The difference between the $(LAO)_{4.5}/(KNO)_{8.5}$ and $(LAO)_5/(KNO)_8$ superlattices is that $(AlO)^-$ is replaced with $(NbO)^+$. We used IF-1, and IF-2 to represent the first, and second NbO_2 monolayers, respectively. The metallic states originate from the Nb 4d orbitals in the IF-1 and IF-2 NbO_2 layers, but without LAO contribution, demonstrating that the "extra" electrons are shared by Nb atoms. In terms of the spatial extension of the 2DEG in the NP-SL and NN-SL, the former has electrons confined to IF-1 near the Fermi level, while the latter shows a greater depth of 2DEG formation. In addition, unlike the O 2p and Nb 4d states shifting to the Fermi level in the NP-SL, these states are almost identical for the layers away from the interface of $(LaO)^+/(NbO_2)^+$ in the NN-SL because of symmetrical polar layers.

The orbital-resolved partial DOS of Nb 4d orbitals (IF-1 and IF-2) are shown in Fig. 5(b), indicating that the half-metallic states at the IF-1 NbO_2 layer are all from d_{xy} orbitals with a local magnetic moment of about 0.50 μ_B on Nb 4d orbitals due to the exchange splitting of the Nb 4d states at the interface, while the IF-2 layer does not have half-metallic states and its metallic states are from d_{xy} and d_{yz} orbitals. Comparing with the NP-SL, there exists only the 2DEG in the NN-SL of polar/polar LAO/KNO superlattices and the 2DEG with full spin polarization can be produced at the interfacial $(NbO_2)^+$ monolayer which is interesting for spintronics applications.
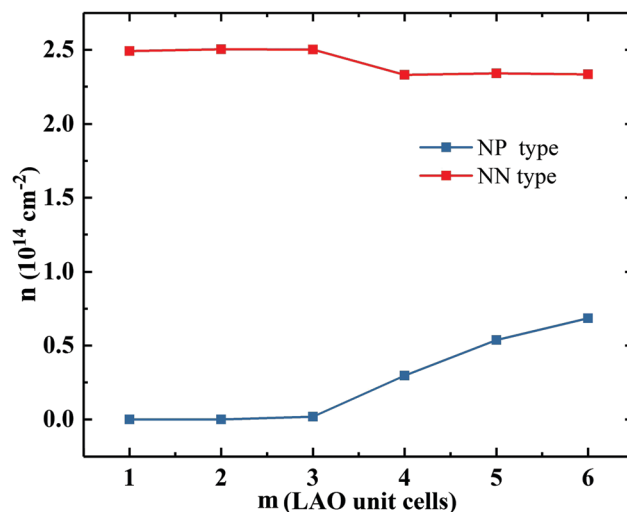

Fig. 6 Calculated interfacial charge carrier density for the stoichiometric NP type of $(LaAlO_3)_m/(KNbO_3)_8$ and the non-stoichiometric NN type of $(LaAlO_3)_m/(KNbO_3)_{8.5}$ superlattices as a function of the number of $LaAlO_3$ unit cells.

4. Interfacial charge carrier density

Because the interfacial charge carrier density plays an important role in determining the conductivity of the LAO/KNO superlattices, we calculated the occupation of Nb 4d orbitals in the NbO$_2$ layer (IF-1) *via* integrating the partial DOS near the Fermi level, and display the relation between the interfacial charge carrier density and the parameter m, as shown in Fig. 6.

For the NP-SL of LAO/KNO superlattices, the magnitude of interfacial charge carrier density is of the order 10^{13} cm^{-2}, while it is 10^{14} cm^{-2} for the NN-SL, since there are extra electrons in the NN-SL because of the non-stoichiometric structure. For the former, when $m = 3$, the interfacial charge carrier density is produced, which then increased from 0.175×10^{13} cm^{-2} to 5.692×10^{13} cm^{-2} with m increasing from 3 to 6. It shows a trend of proportional growth in this thickness range. Therefore, it is possible to adjust the interfacial charge carrier density by changing the number of LAO unit cells for the NP-SL of LAO/KNO superlattices. For the NN case, the interfacial charge carrier density remains around 2.4×10^{14} cm^{-2}, and such a high value of concentration is much less dependent on the parameter m.

We also considered carefully the difference of the polarized atomic layer and intrinsic ferroelectric polarization in KNbO$_3$. In detail, we calculated electronic band structures of the unrelaxed (LAO)$_{4.5}$/(KNO)$_{8.5}$ and (LAO)$_5$/(KNO)$_8$ superlattices without intrinsic ferroelectric polarization of KNO due to atomic displacements. We can learn from Fig. S2 (ESI†) that the charge-polarized atomic layer and the ferroelectric polarization undergo opposite effects, *i.e.* the presence of ferroelectricity weakens the concentration of the 2DEG or 2DHG.

5. Electron effective mass and conductivity

In addition to the charge carrier density, the charge carrier mobility is another important factor for determining the interfacial

conductivity. In the Drude model,[17] the charge carrier mobility μ can be obtained from the formula:

$$\mu = e\langle\tau\rangle/m^\star \quad (1)$$

where e is the electronic charge, τ is the scattering time, and $m^\star$ is the effective mass. The scattering time τ is assumed to be a constant, determined by several scattering factors, such as phonon scattering, electron–electron scattering, impurity scattering, and so on.[28,43] It is clear that the effective mass $m^\star$ is an important factor to affect the charge carrier mobility μ. Firstly, we calculated the band structure along the path M–Γ–X in the Brillouin zone of NP type and NN type models,[18] as shown in Fig. 7. In Fig. 7(a), we can see that the majority-spin and minority-spin states of the conduction bands both pass through the Fermi level, which are contributed by Nb 4d$_{xy}$. Moreover, the O 2p states near the valence band edge also cross the Fermi level, from the hole states of (AlO$_2$)$^-$ at the interface. In Fig. 7(b), there are only majority-spin electrons at the bottom conduction bands passing through the Fermi level, which are composed of Nb d$_{xy}$ orbitals, resulting in the spin-polarized 2DEG at the interface.

Then we calculated electron relative mass $m^\star/m_e$ along the Γ–X and Γ–M directions using the bottom conduction band for the superlattices, in which m_e is the free electron mass. The effective mass $m^\star$ was calculated by the formula:

$$\frac{1}{m^\star} = \frac{1}{\hbar^2}\frac{\partial^2 E_{CB}}{\partial k^2} \quad (2)$$

where $\hbar$ is the reduced Planck constant, E_{CB} is the energy of the minimum conduction band and k is the wave vector related to the conduction band. The calculated relative effective masses

Table 1 Calculated relative electron effective mass $m^\star/m_e$ along Γ–X and Γ–M paths for (LaAlO$_3$)$_5$/(KNbO$_3$)$_8$ and (LaAlO$_3$)$_{4.5}$/(KNbO$_3$)$_{8.5}$ superlattices

Systems	$m^\star/m_e$	
	Γ–X	Γ–M
(LaAlO$_3$)$_5$/(KNbO$_3$)$_8$	0.239	0.240
(LaAlO$_3$)$_{4.5}$/(KNbO$_3$)$_{8.5}$	0.184	0.185
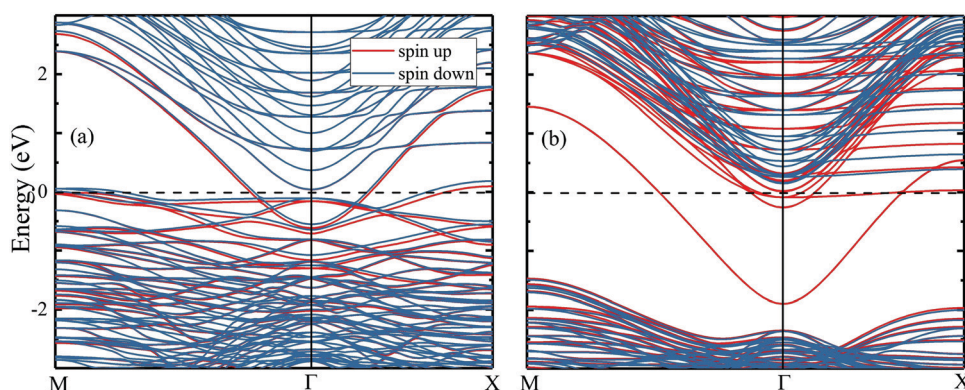
Fig. 7 Electronic band structures for the (a) NP type of (LaAlO$_3$)$_5$/(KNbO$_3$)$_8$ and (b) NN type of (LaAlO$_3$)$_{4.5}$/(KNbO$_3$)$_{8.5}$ superlattices, respectively. The red (blue) lines indicate the majority (minority)-spin states, and the black horizontal dashed line at 0 eV indicates the Fermi level. The bottom conduction band is employed to calculate the relative electron effective mass.

along the Γ–X and Γ–M directions for the superlattices are listed in Table 1. From this comparison, we can find that the $(LaAlO_3)_{4.5}/(KNbO_3)_{8.5}$ system has a smaller effective mass than the $(LaAlO_3)_5/(KNbO_3)_8$ system.

6. Conclusion

In summary, spin-polarized density functional theory calculations are employed to investigate the electronic properties of the stoichiometric NP type model and non-stoichiometric NN type model of LAO/KNO superlattices. For the former, there exists a critical LAO thickness of 3 unit cells for an insulator-to-metal transition, and there is a coexistence of a 2DEG from Nb $4d_{xy}$ orbitals and a 2DHG from O $2p_z$ orbitals. Unlike the case of NP type models, the NN type models show no critical thickness, and the interfacial metallic states from Nb $4d_{xy}$ orbitals are found to be independent of the LAO thickness. In particular, we selected $(LAO)_5/(KNO)_8$ and $(LAO)_{4.5}/(KNO)_{8.5}$ superlattices to show their interfacial charge carrier densities and electron effective masses. The $(LAO)_{4.5}/(KNO)_{8.5}$ superlattice shows a much higher interfacial charge carrier density and a smaller electron effective mass than the $(LAO)_5/(KNO)_8$ superlattice. In conclusion, our investigation revealed the difference of interfacial properties between two different superlattice setups in the polar/polar LAO/KNO systems. This provides fundamental insights into the different interfacial electronic properties and the primary mechanism responsible for the formation of a 2DEG in polar/polar NP and NN type LAO/KNO superlattices.

Conflicts of interest

The authors declare no competing financial interest.

Acknowledgements

References

1 A. Brinkman, M. Huijben, M. van Zalk, J. Huijben, U. Zeitler, J. C. Maan, W. G. van der Wiel, G. Rijnders, D. H. A. Blank and H. Hilgenkamp, Magnetic effects at the interface between non-magnetic oxides, *Nat. Mater.*, 2007, **6**, 493–496.

2 J. B. Neaton and K. M. Rabe, Theory of polarization enhancement in epitaxial BaTiO$_3$/SrTiO$_3$ superlattices, *Appl. Phys. Lett.*, 2003, **82**, 1586–1588.

3 S. Thiel, G. Hammerl, A. Schmehl, C. W. Schneider and J. Mannhart, Tunable Quasi-Two-Dimensional Electron Gases in Oxide Heterostructures, *Science*, 2006, 1942–1944.

4 N. Reyren, S. Thiel, A. D. Caviglia, L. F. Kourkoutis, G. Hammerl, C. Richter, C. W. Schneider, T. Kopp, A.-S. Rüetschi, D. Jaccard, M. Gabay, D. A. Muller, J.-M. Triscone and J. Mannhart, Superconducting Interfaces Between Insulating Oxides, *Science*, 2007, **317**, 1196–1199.

5 L. Weston, X. Y. Cui, S. P. Ringer and C. Stampfl, Density-Functional Prediction of a Surface Magnetic Phase in SrTiO$_3$/LaAlO$_3$ Heterostructures Induced by Al Vacancies, *Phys. Rev. Lett.*, 2014, **113**, 186401.

6 R. Pentcheva and W. E. Pickett, Avoiding the Polarization Catastrophe in LaAlO$_3$ Overlayers on SrTiO$_3$ (001) through Polar Distortion, *Phys. Rev. Lett.*, 2009, **102**, 107602.

7 K. D. Fredrickson and A. A. Demkov, Switchable conductivity at the ferroelectric interface: Nonpolar oxides, *Phys. Rev. B: Condens. Matter Mater. Phys.*, 2015, **91**, 115126.

8 A. Ohtomo and H. Y. Hwang, A high-mobility electron gas at the LaAlO$_3$/SrTiO$_3$ heterointerface, *Nature*, 2004, **427**, 423–426.

9 N. Nakagawa, H. Y. Hwang and D. A. Muller, Why some interfaces cannot be sharp, *Nat. Mater.*, 2006, **5**, 204–209.

10 W. A. Harrison, E. A. Kraut, J. R. Waldrop and R. W. Grant, Polar heterojunction interfaces, *Phys. Rev. B: Condens. Matter Mater. Phys.*, 1978, **18**, 4402–4410.

11 G. A. Baraff, J. A. Appelbaum and D. R. Hamann, Self-Consistent Calculation of the Electronic Structure at an Abrupt GaAs-Ge Interface, *Phys. Rev. Lett.*, 1977, **38**, 237–240.

12 H. Chen, A. M. Kolpak and S. Ismail-Beigi, Fundamental asymmetry in interfacial electronic reconstruction between insulating oxides: An ab initio study, *Phys. Rev. B: Condens. Matter Mater. Phys.*, 2009, **79**, 161402.

13 J. A. Sulpizio, S. Ilani, P. Irvin and J. Levy, Nanoscale Phenomena in Oxide Heterostructures, *Ann. Rev. Mater. Res.*, 2014, **44**, 117–149.

14 L. Yu and A. Zunger, A polarity-induced defect mechanism for conductivity and magnetism at polar-nonpolar oxide interfaces, *Nat. Commun.*, 2014, **5**, 5118.

15 A. Kalabukhov, R. Gunnarsson, J. Börjesson, E. Olsson, T. Claeson and D. Winkler, Effect of oxygen vacancies in the SrTiO$_3$ substrate on the electrical properties of the LaAlO$_3$/SrTiO$_3$ interface, *Phys. Rev. B: Condens. Matter Mater. Phys.*, 2007, **75**, 121404.

16 R. Dingle, H. L. Störmer, A. C. Gossard and W. Wiegmann, Electron mobilities in modulation-doped semiconductor heterojunction superlattices, *Appl. Phys. Lett.*, 1978, **33**, 665–667.

17 K. Zou, S. Ismail-Beigi, K. Kisslinger, X. Shen, D. Su, F. J. Walker and C. H. Ahn, LaTiO$_3$/KTaO$_3$ interfaces: A new two-dimensional electron gas system, *APL Mater.*, 2015, **3**, 036104.

18 Y. Wang, W. Tang, J. Cheng, M. Behtash and K. Yang, Creating a Two-Dimensional Electron Gas in Polar/Polar

8052 | *Phys. Chem. Chem. Phys.*, 2019, **21**, 8046–8053

This journal is © the Owner Societies 2019

Perovskite Oxide Heterostructures: First-Principles Characterization of LaAlO$_3$/A$^+$B^{5+}O$_3$, *ACS Appl. Mater. Interfaces*, 2016, **8**, 13659–13668.

19 J. Li, W. Wu, Y. Shen, P. Zhang, Y. Hong, H. Bai, G. Li and Z. Zhou, From LaAlO$_3$/SrTiO$_3$ to LaAlO$_3$/KNbO$_3$: Improving the transport properties of a two-dimensional electronic gas in created +1/+1 interfaces, *Comput. Mater. Sci.*, 2019, **156**, 286–291.

20 L. Yin, W. Mi and X. Wang, Prediction of a metal–insulator transition and a two-dimensional electron gas in ortho-ferrite LaTiO$_3$/tetragonal BiFeO$_3$ heterostructures, *J. Mater. Chem. C*, 2015, **3**(42), 11066–11075.

21 J. Liu, G. Chen, Z. Li and Z. Zhang, Hydrothermal synthesis and photocatalytic properties of ATaO$_3$ and ANbO$_3$ (A = Na and K), *Int. J. Hydrogen Energy*, 2007, **32**, 2269–2272.

22 N. Kumada, T. Kyoda, Y. Yonesaki, T. Takei and N. Kinomura, Preparation of KNbO$_3$ by hydrothermal reaction, *Mater. Res. Bull.*, 2007, **42**, 1856–1862.

23 S. A. Hayward, F. D. Morrison, S. A. T. Redfern, E. K. H. Salje, J. F. Scott, K. S. Knight, S. Tarantino, A. M. Glazer, V. Shuvaeva, P. Daniel, M. Zhang and M. A. Carpenter, Transformation processes in LaAlO$_3$: Neutron diffraction, dielectric, thermal, optical, and Raman studies, *Phys. Rev. B: Condens. Matter Mater. Phys.*, 2005, **72**, 054110.

24 J. Cheng, S. Nazir and K. Yang, First-Principles Prediction of a Two-Dimensional Electron Gas Driven by Polarization Discontinuity in Nonpolar/Nonpolar AHfO$_3$/SrTiO$_3$ (A = Ca, Sr, and Ba) Heterostructures, *ACS Appl. Mater. Interfaces*, 2016, **8**, 31959–31967.

25 L. Li, B. J. Kennedy, Y. Kubota, K. Kato and R. F. Garrett, Structures and phase transitions in Sr$_{1-x}$Ba$_x$HfO$_3$ perovskites, *J. Mater. Chem.*, 2004, **14**, 263–273.

26 M. J. Nystrom, B. W. Wessels, D. B. Studebaker, T. J. Marks, W. P. Lin and G. K. Wong, Epitaxial potassium niobate thin films prepared by metalorganic chemical vapor deposition, *Appl. Phys. Lett.*, 1995, **67**, 365–367.

27 M. J. Nystrom, B. W. Wessels, J. Chen and T. J. Marks, Microstructure of epitaxial potassium niobate thin films prepared by metalorganic chemical vapor deposition, *Appl. Phys. Lett.*, 1996, **68**, 761–763.

28 M. C. Karamargin, C. A. Reynolds, F. P. Lipschultz and P. G. Klemens, Lattice Thermal Conductivity and Deviations from Matthiessen's Rule for Dilute Alloys of Tin with Cadmium, *Phys. Rev. B: Solid State*, 1972, **6**, 3624–3633.

29 G. F. Keresse, Efficient Iterative Schemes for Ab Initio Total-Energy Calculations Using a Plane-Wave Basis Set, *Phys. Rev. B: Condens. Matter Mater. Phys.*, 1996, **54**, 11169–11186.

30 J. P. Perdew, K. Burke and M. Ernzerhof, Generalized Gradient Approximation Made Simple, *Phys. Rev. Lett.*, 1996, **77**, 3865–3868.

31 V. R. Cooper, Enhanced carrier mobilities in two-dimensional electron gases at III–III/I–V oxide heterostructure interfaces, *Phys. Rev. B: Condens. Matter Mater. Phys.*, 2012, **85**, 235109.

32 R. Pentcheva and W. E. Pickett, Ionic relaxation contribution to the electronic reconstruction at the n-type LaAlO$_3$/SrTiO$_3$ interface, *Phys. Rev. B: Condens. Matter Mater. Phys.*, 2008, **78**, 205106.

33 M. Gu, J. Wang, X. S. Wu and G. P. Zhang, Stabilities of the Intrinsic Defects on SrTiO$_3$ Surface and SrTiO$_3$/LaAlO$_3$ Interface, *J. Phys. Chem. C*, 2012, **116**(47), 24993–24998.

34 Y. Wang, M. K. Niranjan, S. S. Jaswal and E. Y. Tsymbal, First-principles studies of a two-dimensional electron gas at the interface in ferroelectric oxide heterostructures, *Phys. Rev. B: Condens. Matter Mater. Phys.*, 2009, **80**, 16.

35 N. C. Bristowe, E. Artacho and P. B. Littlewood, Oxide superlattices with alternating p and n interfaces, *Phys. Rev. B: Condens. Matter Mater. Phys.*, 2009, **80**(4), 045425.

36 H. Chen, A. M. Kolpak and S. Ismail-Beigi, Electronic and magnetic properties of SrTiO$_3$/LaAlO$_3$ interfaces from first principles, *Adv. Mater.*, 2010, **22**(26-27), 2881–2899.

37 P. X. Zhou, S. Dong, H. M. Liu, C. Y. Ma, Z. B. Yan, C. G. Zhong and J. M. Liu, Ferroelectricity driven magnetism at domain walls in LaAlO$_3$/PbTiO$_3$ superlattices, *Sci. Rep.*, 2015, **5**, 13052.

38 Y. Z. Chen, F. Trier, T. Wijnands, R. J. Green, N. Gauquelin, R. Egoavil, D. V. Christensen, G. Koster, M. Huijben, N. Bovet, S. Macke, F. He, R. Sutarto, N. H. Andersen, J. A. Sulpizio, M. Honig, G. E. D. K. Prawiroatmodjo, T. S. Jespersen, S. Linderoth, S. Ilani, J. Verbeeck, G. Van Tendeloo, G. Rijnders, G. A. Sawatzky and N. Pryds, Extreme mobility enhancement of two-dimensional electron gases at oxide interfaces by charge-transfer-induced modulation doping, *Nat. Mater.*, 2015, **14**, 801–806.

39 C. Cen, S. Thiel, G. Hammerl, C. W. Schneider, K. E. Andersen, C. S. Hellberg, J. Mannhart and J. Levy, Nanoscale control of an interfacial metal-insulator transition at room temperature, *Nat. Mater.*, 2008, **7**, 298–302.

40 M. Behtash, S. Nazir, Y. Wang and K. Yang, Polarization effects on the interfacial conductivity in LaAlO$_3$/SrTiO$_3$ heterostructures: a first-principles study, *Phys. Chem. Chem. Phys.*, 2016, **18**, 6831–6838.

41 F. Wang, Z. Ren, H. Tian, S. A. Yang, Y. Xie, Y. Lu, J. Jiang, G. Han and K. Yang, Interfacial Multiferroics of TiO$_2$/PbTiO$_3$ Heterostructure Driven by Ferroelectric Polarization Discontinuity, *ACS Appl. Mater. Interfaces*, 2017, **9**, 1899–1906.

42 Y. Wang, M. K. Niranjan, J. D. Burton, J. M. An, K. D. Belashchenko and E. Y. Tsymbal, Prediction of a spin-polarized two-dimensional electron gas at the LaAlO$_3$/EuO (001) interface, *Phys. Rev. B: Condens. Matter Mater. Phys.*, 2009, **79**, 212408.

43 C. Chen, L. Fang, J. Zhang, G. Zhao and W. Ren, Thickness Control of the Spin-Polarized Two-Dimensional Electron Gas in LaAlO$_3$/BaTiO$_3$ Superlattices, *Sci. Rep.*, 2018, **8**, 467.

This journal is © the Owner Societies 2019

Phys. Chem. Chem. Phys., 2019, **21**, 8046–8053 | **8053**